Using normative models pre-trained on cross-sectional data to evaluate longitudinal changes in neuroimaging data

Barbora Rehák Bučková[1,2,3], Charlotte Fraza[4], Rastislav Rehák[5,6], Marián Kolenič[3], Christian Beckmann[4], Filip Španiel[3], Andre Marquand[4†], and Jaroslav Hlinka[1,3†]

[1]Department of Complex Systems, Institute of Computer Science of the Czech Academy of Sciences, Prague, Czech Republic

[2]Department of Cybernetics, Czech Technical University in Prague, Prague, Czech Republic

[3]National Institute of Mental Health, Klecany, Czech Republic

[4]Donders Institute for Brain, Cognition and Behaviour, Nijmegen, Netherlands

[5]Max Planck Institute for Research on Collective Goods, Bonn, Germany

[6]University of Cologne, Germany

[*]Corresponding author. Email: andre.marquand@donders.ru.nl, hlinka@cs.cas.cz

[†]These authors contributed equally to this work.

Abstract

Longitudinal neuroimaging studies offer valuable insight into intricate dynamics of brain development, ageing, and disease progression over time. However, prevailing analytical approaches rooted in our understanding of population variation are primarily tailored for cross-sectional studies. To fully harness the potential of longitudinal neuroimaging data, we have to develop and refine methodologies that are adapted to longitudinal designs, considering the complex interplay between population variation and individual dynamics.

We build on normative modelling framework, which enables the evaluation of an individual's position compared to a population standard. We extend this framework to evaluate an individual's *change* compared to standard dynamics. Thus, we exploit the existing normative models pre-trained on over 58,000 individuals and adapt the framework so that they can also be used in the evaluation of longitudinal studies. Specifically, we introduce a quantitative metric termed *"z-diff"* score, which serves as an indicator of change of an individual compared to a population standard. Notably, our framework offers advantages such as flexibility in dataset size and ease of implementation.

To illustrate our approach, we applied it to a longitudinal dataset of 98 patients diagnosed with early-stage schizophrenia who underwent MRI examinations shortly after diagnosis and one year later.

Compared to cross-sectional analyses, which showed global thinning of grey matter at the first visit, our method revealed a significant normalisation of grey matter thickness in the frontal lobe over time. Furthermore, this result was not observed when using more traditional methods of longitudinal analysis, making our approach more sensitive to temporal changes.

Overall, our framework presents a flexible and effective methodology for analysing longitudinal neuroimaging data, providing insights into the progression of a disease that would otherwise be missed when using more traditional approaches.

1 Introduction

Longitudinal neuroimaging studies provide a unique opportunity to gain insight into the temporal dynamics of a disease, over and above the insights offered by cross-sectional studies. Efforts related to the acquisition of these datasets are non-trivial and require substantial time and funding while accounting for problems inherent to longitudinal studies such as the dropout of subjects between time points, standardisation over multiple clinical centres, and changes in imaging technology over time. Considering this challenging task, it is of great consequence to have tools to effectively analyse them whilst also making use of more widely available cross-sectional data to refine inferences.

Despite the significance of longitudinal data analysis and the need for appropriate tools, there is a notable shortage of suitable methods and their development lacks behind. Even though recent advances in the acquisition and publication of large neuroimaging datasets [1, 2] have significantly improved our understanding of population variation, the developed methodologies are largely focused on the cross-sectional nature of the data [3]. Indeed, these methods are essential for characterising an individual's position in a population; however, the vital factor of longitudinal change is largely neglected. Consequently, efforts should be made to tailor the standing methods modelling population variation for a longitudinal context to advance our understanding of disease progression. This endeavour would create an alternative to the widely used mixed-effect models [4], which may suffer from poor out-of-sample prediction and struggle with accommodating non-linear lifespan trajectories.

Among the promising cross-sectional techniques for modelling population variation, which emerged in recent years, is normative modelling [5, 6]. This framework models each image-derived phenotype (IDP) (i.e., voxel intensity, regional average, or regional volume) independently as a function of clinical variables (e.g., age, sex, scanning site) in a large healthy population. Subjects are subsequently compared to the healthy population, which enables us to evaluate the position of each individual, rather than just compare group differences between patients and controls [7, 8]. Application of these models has already provided valuable insights into the individual neuroanatomy of various diseases, such as Alzheimer's, schizophrenia, autism, and other neurological and mental disorders [9–12].

Longitudinal studies are conceptually well suited for normative modelling since

they analyse individual trajectories over time. If adjusted appropriately, normative models could not only improve predictive accuracy but also identify patterns of change, thereby enhancing our understanding of the disease. In contrast to traditional statistical methods that estimate the average change in the group, normative models could estimate individual deviations from healthy trajectories. This comprehensive approach would take into account both population heterogeneity and confounders, thus providing a more nuanced understanding of change over time.

Normative modelling is a relatively new area of research and thus, despite its potential, longitudinal normative models have not been systematically explored [6, 13]. Indeed, virtually all large-scale normative models released to date are estimated on cross-sectional data [6, 14] and a recent report [13] has provided empirical data to suggest that such cross-sectional models may underestimate the variance in longitudinal data [13]. However, from a theoretical perspective, it is very important to recognise that cross-sectional models describe group-level population variation across the lifespan, where such group level centiles are interpolated smoothly across time. It is well-known in the pediatric growth-charting literature (e.g. [15]) that centiles in such cross-sectional models do not necessarily correspond to individual level trajectories, rather it is possible that individuals cross multiple centiles as they proceed through development, even in the absence of pathology. Crucially, classical growth charts, and current normative brain charts provide no information about how frequent such centile crossings are in general. In other words, they provide a *trajectory of distributions*, **not** a *distribution over trajectories*. There are different approaches to tackle this problem in the growth charting literature, including the estimation of 'thrive lines' that map centiles of constant velocity across the lifespan and can be used to declare 'failure to thrive' at the individual level (see e.g. [15] for details). Unfortunately, this approach requires densely sampled longitudinal neuroimaging data to estimate growth velocity, that are not available across the human lifespan at present. Therefore, in this work, we adopt a different approach based on estimates of the uncertainty in the centile estimates themselves together with the uncertainty with which a point is measured (e.g. bounded by the test-retest reliability, noise etc.). By accounting for such variability, this provides a statistic to determine whether a centile crossing is large enough to be statistically different from the base level within the population.

We stress that our aim is not to build a longitudinal normative model *per se*.

Considering the much greater availability of cross-sectional data relative to longitudinal data, we instead leverage existing models constructed from densely sampled cross-sectional populations and provide methods for applying these to longitudinal cohorts. We argue that although these models lack explicit intra-subject dynamics, they contain sufficient information to enable precise assessments of changes over time. Nevertheless, the inclusion of longitudinal data into existing models largely estimated from cross-sectional data is also an important goal and can be approached with hierarchical models [16]; however, we do not tackle this problem here.

Our approach requires (i) a probabilistic framework to coherently manage uncertainty and (ii) cross-sectional models estimated on large reference cohort to accurately estimate population centiles. To this end, we utilise the Warped Bayesian Linear Regression normative model [7] as a basis for our work. Training these models requires significant amounts of data and computational resources, limiting their use for smaller research groups. However, the availability of pre-trained models has made them more accessible to researchers from a wider range of backgrounds, as reported by Rutherford et al. [14].

In summary, in this work, we propose a framework for using pre-trained normative models derived from cross-sectional data to evaluate longitudinal studies. We briefly present the existing model and derive a novel set of difference ("*z-diff*") scores for statistical evaluation of change between measurements. We then describe its implementation and showcase its practical application to an in-house longitudinal dataset of 98 patients in the early stages of schizophrenia who underwent fMRI examinations shortly after being diagnosed and one year after.

2 Methods

2.1 Model formulation

2.1.1 Original model for cross-sectional data

Here, we briefly present the original normative model [7], developed to be trained and used on cross-sectional data. In the following subsection, we take this model pre-trained on a large cross-sectional database, and extend it so that it can be used on longitudinal data.

The original model [7] is pre-trained on a cross-sectional database $\mathbf{Y} = (y_{nd}) \in$

$\mathbb{R}^{N\times D}$, $\mathbf{X} = (x_{nm}) \in \mathbb{R}^{N\times M}$ of N subjects, for whom we observe D IDPs and M covariates (e.g., age or sex). Thus, y_{nd} is the d-th IDP of the n-th subject and x_{nm} is the m-th covariate of the n-th subject.

Since each IDP is treated separately, we focus on a fixed IDP d and drop this index for ease of exposition. To simplify notation, we denote $\mathbf{y} = (y_1, \ldots, y_N)^T$ the column of observations of this fixed IDP across subjects. The observations are assumed to be independent (across n). To model the relationship between IDP y_n and covariates $\mathbf{x}_n = (x_{n1}, \ldots, x_{nM})^T$, we want to exploit a normal linear regression model. However, we make a couple of adjustments first:

- To accommodate non-Gaussian errors in the original space of dependent variables, we transform the original variable y_n by a warping function $\varphi(y_n)$, which is parametrised by hyper-parameters $\boldsymbol{\gamma}$ (see [7] for technical details).

- To capture non-linear relationships, we use a common B-spline basis expansion of the original independent variables $\mathbf{x}_n$ (see [7] for technical details). To accommodate site-level effects, we append it with site dummies. We denote the resulting transformation of $\mathbf{x}_n$ $\phi(\mathbf{x}_n) \in \mathbb{R}^K$.

We also treat the precision of measurements as a hyper-parameter and we denote it by β. Thus, we model the distribution of the transformed IDP $\varphi(y_n)$ conditional on covariates $\mathbf{x}_n$, vector of parameters $\mathbf{w}$, and hyper-parameters β and $\boldsymbol{\gamma}$ as

$$\varphi(y_n)|\mathbf{x}_n; \mathbf{w}; \beta, \boldsymbol{\gamma} \sim \mathcal{N}(\mathbf{w}^T\phi(\mathbf{x}_n), \beta^{-1}). \tag{1}$$

We write this as

$$\varphi(y_n) = \mathbf{w}^T\phi(\mathbf{x}_n) + \varepsilon_n,\ \varepsilon_n \sim \mathcal{N}(0, \beta^{-1}), \tag{2}$$

where ε_n are independent from $\mathbf{x}_n$ and across n. In practical terms, ε_n represents the deviation of subject n from the population mean, together with the measurement error. We further denote $\boldsymbol{\Lambda}_\beta = \beta\mathbf{I} \in \mathbb{R}^{N\times N}$ and the design matrix $\boldsymbol{\Phi} = (\phi(\mathbf{x}_n)_k) \in \mathbb{R}^{N\times K}$ ($\phi(\mathbf{x}_n)_k$ is the k-the element of vector $\phi(\mathbf{x}_n)$).

The estimation of parameters $\mathbf{w}$ is performed by empirical Bayesian methods. In particular, prior about $\mathbf{w}$

$$\mathcal{N}(0, \boldsymbol{\Lambda}_\alpha^{-1}),\ \boldsymbol{\Lambda}_\alpha = \alpha\mathbf{I} \tag{3}$$

is combined with the likelihood function to derive the posterior

$$\mathbf{w}|\mathbf{y}, \mathbf{\Phi}; \alpha, \beta, \boldsymbol{\gamma} \sim \mathcal{N}(\bar{\mathbf{w}}, \mathbf{A}^{-1}), \tag{4}$$

$$\mathbf{A} = \mathbf{\Phi}^T \mathbf{\Lambda}_\beta \mathbf{\Phi} + \mathbf{\Lambda}_\alpha, \tag{5}$$

$$\bar{\mathbf{w}} = \mathbf{A}^{-1} \mathbf{\Phi}^T \mathbf{\Lambda}_\beta \mathbf{y}. \tag{6}$$

The hyper-parameters $\alpha, \beta, \boldsymbol{\gamma}$ are estimated by maximising the warped marginal log-likelihood.

The predictive distribution of $\varphi(y)$ for a subject with $\mathbf{x}$ is

$$\mathcal{N}(\bar{\mathbf{w}}^T \phi(\mathbf{x}), \phi(\mathbf{x})^T \mathbf{A}^{-1} \phi(\mathbf{x}) + \beta^{-1}). \tag{7}$$

Hence, the z-score characterising the position of this subject within population is

$$z = \frac{\varphi(y) - \bar{\mathbf{w}}^T \phi(\mathbf{x})}{\sqrt{\phi(\mathbf{x})^T \mathbf{A}^{-1} \phi(\mathbf{x}) + \beta^{-1}}}, \tag{8}$$

where $\varphi(y)$ is the realised warped observation of IDP d for this subject.

Note that formulae (7) and (8) implicitly evaluate only (potentially new) subjects measured at sites already present in the original database $\mathbf{y}$, $\mathbf{\Phi}$. If we want to evaluate subjects measured at a new site, we will have to run an adaptation procedure to account for its effect. This adaptation procedure is described and readily accessible online in [14]. In short, a sample of a reference (healthy) cohort measured on the same scanner as the population of interest is needed to accommodate a site-specific effect.

In the following section, we develop a procedure that allows to extend the original cross-sectional framework pre-trained on database $\mathbf{y}$, $\mathbf{\Phi}$ to evaluate a new longitudinal dataset for assessment of changes in regional brain thickness.

2.1.2 Adaptation to longitudinal data

We aim to adapt the original framework [7] in order to leverage its parameters pre-trained on a large cross-sectional database $\mathbf{y}$, $\mathbf{\Phi}$. We design a score for a change between visits (further referred to as *z-diff* score), based on which we can detect unusual changes in regional brain thickness. In other words, we extend the existing cross-sectional normative modelling framework to be useful in the evaluation of

longitudinal data.

To utilise the normative model of the healthy population pre-trained on cross-sectional data in the longitudinal setup, we have to make an assumption about the trajectory of healthy controls. The natural first assumption is that a *healthy* subject does not deviate substantially from their position within the population as time progresses, so the observed position changes between the visits of a healthy subject are assumed to stem from observation noise (due to technical or physiological factors) and are therefore constrained by the test-retest reliability of the measurement. Note that this does not imply that a healthy subject does not change over time, but rather that the change follows approximately the centile of distribution at which the individual is placed. We acknowledge that this is a relatively strong assumption, but it is reasonable to assume that a *healthy* subject's brain activity or structure will remain relatively stable over short time periods (years, but not necessarily decades), and any significant changes in the pattern compared to the normative reference database may indicate disease progression or response to intervention [12]. Also, it is very important to recognise that this model does not constrain a given subject to follow a population-level centile trajectory exactly because the model includes an error component (later denoted $\xi^{(i)}$) that allows for individual-level deviations from the population centile.

We connect to the cross-sectional model by invoking the above assumption through reinterpretation of the error term $\varepsilon \sim \mathcal{N}(0, \beta^{-1})$. In particular, we decompose it to a subject-specific factor η and a measurement error $\xi^{(i)}$ in the i-th visit. While η is considered constant across the visits (of a healthy cohort subject) and captures the subject's position within the population, $\xi^{(i)}$ is specific for the i-th visit and captures a combination of movement, acquisition, processing noise, etc. Hence, the model for the i-th visit of a subject with given covariates $\mathbf{x}^{(i)}$ is

$$\begin{aligned} \varphi(y^{(i)}) &= \mathbf{w}^T \phi(\mathbf{x}^{(i)}) + \eta + \xi^{(i)} \\ \eta &\sim \mathcal{N}(0, \sigma_\eta^2) \\ \xi^{(i)} &\sim \mathcal{N}(0, \sigma_\xi^2) \\ \beta^{-1} &= \sigma_\eta^2 + \sigma_\xi^2 \end{aligned} \tag{9}$$

where η, $\xi^{(i)}$, and $\mathbf{x}^{(i)}$ are mutually independent for a given i, and the measurement errors $\xi^{(i)}$ and $\xi^{(j)}$ are independent across visits $i \neq j$. Note that we dropped the subject-specific index n used in (1). This should force the reader to distinguish

between the data used for training the original model and a new set of longitudinal data, in which we want to evaluate the longitudinal change of subjects.

In our longitudinal data, we are interested in the change for a given individual across two visits. According to model (9), the difference in the transformed IDP between visits 1 and 2, $\varphi(y^{(2)}) - \varphi(y^{(1)})$, for a subject with covariates $\mathbf{x}^{(1)}$ and $\mathbf{x}^{(2)}$ is given by

$$\varphi(y^{(2)}) - \varphi(y^{(1)}) = \mathbf{w}^T[\phi(\mathbf{x}^{(2)}) - \phi(\mathbf{x}^{(1)})] + \xi^{(2)} - \xi^{(1)} \tag{10}$$

with $\xi^{(2)} - \xi^{(1)} \sim \mathcal{N}(0, 2\sigma_\xi^2)$. We use the posterior distribution of $\mathbf{w}$ with hyper-parameters $\alpha, \beta, \boldsymbol{\gamma}$ estimated on the original cross-sectional database $\mathbf{y}, \boldsymbol{\Phi}$ (the estimates are available at `https://github.com/predictive-clinical-neuroscience/braincharts`). Therefore, the posterior predictive distribution for the difference $\varphi(y^{(2)}) - \varphi(y^{(1)})$ for our subject is (for more detailed derivation, please refer to the supplement)

$$\mathcal{N}\left(\bar{\mathbf{w}}^T[\phi(\mathbf{x}^{(2)}) - \phi(\mathbf{x}^{(1)})], [\phi(\mathbf{x}^{(2)}) - \phi(\mathbf{x}^{(1)})]^T\mathbf{A}^{-1}[\phi(\mathbf{x}^{(2)}) - \phi(\mathbf{x}^{(1)})] + 2\sigma_\xi^2\right). \tag{11}$$

Hence, the z-score for the difference in the transformed IDP between visits 1 and 2 is

$$z\text{-}\mathit{diff} = \frac{[\varphi(y^{(2)}) - \varphi(y^{(1)})] - \bar{\mathbf{w}}^T[\phi(\mathbf{x}^{(2)}) - \phi(\mathbf{x}^{(1)})]}{\sqrt{[\phi(\mathbf{x}^{(2)}) - \phi(\mathbf{x}^{(1)})]^T\mathbf{A}^{-1}[\phi(\mathbf{x}^{(2)}) - \phi(\mathbf{x}^{(1)})] + 2\sigma_\xi^2}}, \tag{12}$$

where $\varphi(y^{(2)}) - \varphi(y^{(1)})$ is the realised change in the warped observations of the IDP for this subject. Since this *z-diff* score is standard normal for the population of healthy controls, any large deviations may be used to detect suspicious changes.

The primary role of adaptation of the pre-trained cross-sectional model to longitudinal data is to account for the measurement noise variance σ_ξ^2. From the posterior predictive distribution (11), we have (denoting the set of conditionals $\Omega = \{\mathbf{x}^{(1)}, \mathbf{x}^{(2)}; \mathbf{y}, \boldsymbol{\Phi}; \alpha, \beta, \boldsymbol{\gamma}\}$)

$$\begin{aligned} &\mathrm{E}\Big[\Big(\varphi(y^{(2)}) - \varphi(y^{(1)}) - \mathrm{E}[\varphi(y^{(2)}) - \varphi(y^{(1)})|\Omega]\Big)^2\Big|\Omega\Big] \\ &\quad = [\phi(\mathbf{x}^{(2)}) - \phi(\mathbf{x}^{(1)})]^T\mathbf{A}^{-1}[\phi(\mathbf{x}^{(2)}) - \phi(\mathbf{x}^{(1)})] + 2\sigma_\xi^2. \end{aligned} \tag{13}$$

Hence, by the Law of Iterated Expectations (to integrate out $\mathbf{x}^{(1)}$ and $\mathbf{x}^{(2)}$), we obtain

$$\mathrm{E}\Big[\Big(\varphi(y^{(2)}) - \varphi(y^{(1)}) - \bar{\mathbf{w}}^T[\phi(\mathbf{x}^{(2)}) - \phi(\mathbf{x}^{(1)})]\Big)^2 \\ - [\phi(\mathbf{x}^{(2)}) - \phi(\mathbf{x}^{(1)})]^T\mathbf{A}^{-1}[\phi(\mathbf{x}^{(2)}) - \phi(\mathbf{x}^{(1)})]\Big|\mathbf{y}, \mathbf{\Phi}; \alpha, \beta, \boldsymbol{\gamma}\Big] = 2\sigma_\xi^2. \tag{14}$$

Therefore, we estimate $2\sigma_\xi^2$ by the sample analogue of the left-hand side in (14). Specifically, we devote a subsample C of our controls to adaptation and we compute

$$\widehat{2\sigma_\xi^2} = \frac{1}{|C|}\sum_{k\in C}\Big[\Big(\varphi(y_k^{(2)}) - \varphi(y_k^{(1)}) - \bar{\mathbf{w}}^T[\phi(\mathbf{x}_k^{(2)}) - \phi(\mathbf{x}_k^{(1)})]\Big)^2 \\ - [\phi(\mathbf{x}_k^{(2)}) - \phi(\mathbf{x}_k^{(1)})]^T\mathbf{A}^{-1}[\phi(\mathbf{x}_k^{(2)}) - \phi(\mathbf{x}_k^{(1)})]\Big]. \tag{15}$$

Moreover, another useful feature of longitudinal data is that $[\phi(\mathbf{x}_k^{(2)}) - \phi(\mathbf{x}_k^{(1)})]$ is negligible (especially with stable covariates, like sex and age). Sex (typically) does not change across the two visits and age relatively little (in our target application) with respect to the full span of ageing. Consequently, $[\phi(\mathbf{x}_k^{(2)}) - \phi(\mathbf{x}_k^{(1)})]^T\mathbf{A}^{-1}[\phi(\mathbf{x}_k^{(2)}) - \phi(\mathbf{x}_k^{(1)})]$ in (15) is negligible in adult cohorts but must be treated with caution in developmental or aging groups. Finally, it is apparent from (5) that $\mathbf{A}$ scales with the number of subjects, and its inverse will be negligible for substantial training datasets, such as the one that was used for pre-training.

To conclude this subsection, we caution against the use of a naive difference of z-scores (instead of *z-diff*) to evaluate the longitudinal change. The problem with such an approach is apparent from (8): it does not properly account for the model uncertainty (the sandwich part with A), and even if the model uncertainty is negligible, it does not properly scale the difference of "residuals" because it ignores the common source of subject-level variability η.

2.1.3 Implementation

To implement the method (Fig. 1), we used the **PCN toolkit**. The exact steps of the analysis with detailed explanations are available in the online tutorial at `PCNtoolkit-demo` (`https://github.com/predictive-clinical-neuroscience/PCNtoolkit-demo`) in the tutorials section.

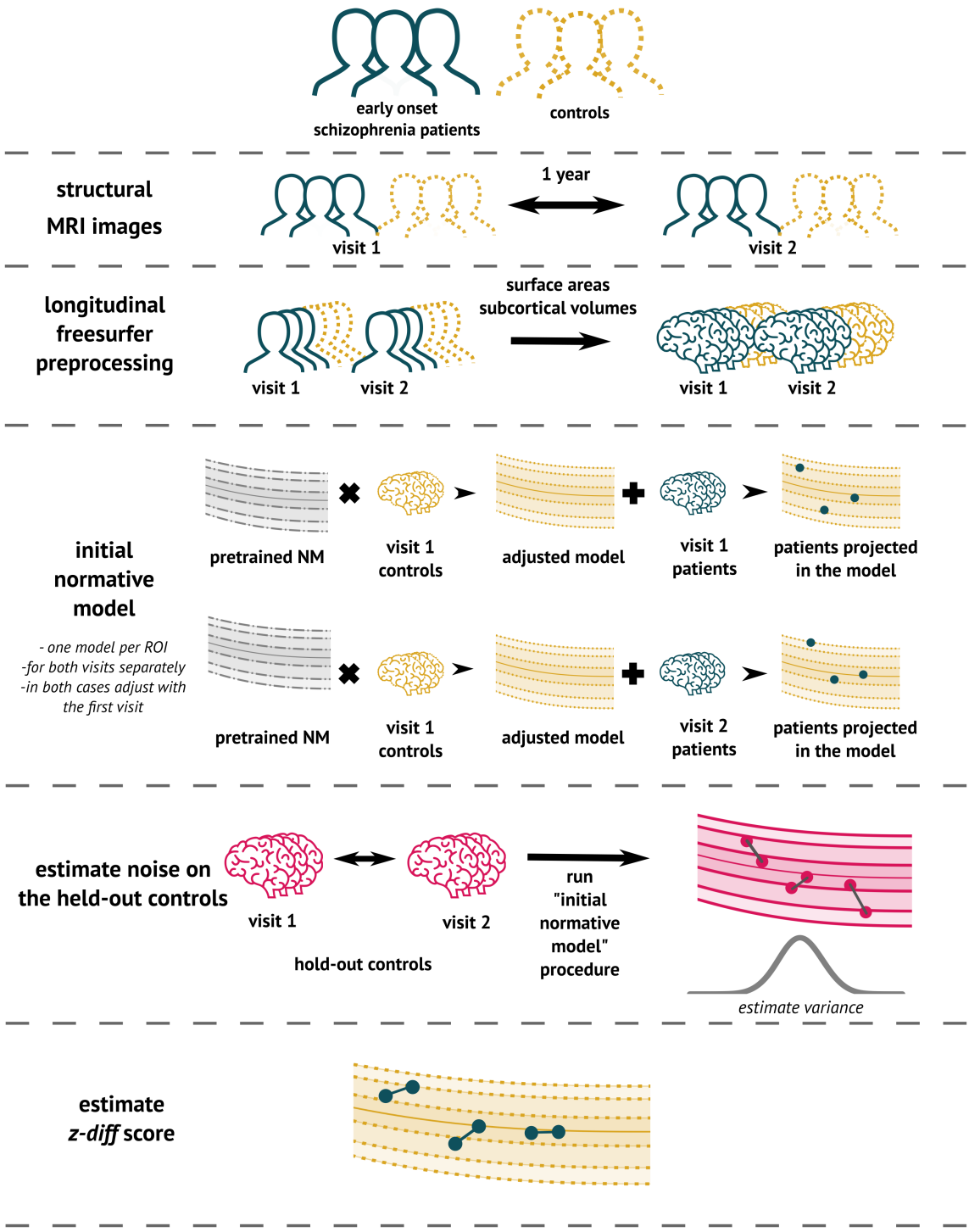

Figure 1: The overview of the analytical pipeline for our schizophrenia patients: First, data are preprocessed using Freesurfer's longitudinal pipeline. Subsequently, the pre-trained models are adjusted to a local sample of healthy controls. The site-specific measurement noise variance σ_ξ^2 in healthy subjects is estimated using held-out controls, and finally, the *z-diff* score is computed.

2.2 Data

2.2.1 Early stages of schizophrenia patients

The clinical data used for the analysis were part of the Early Stages of Schizophrenia study [17]. We analysed data from 98 patients in the early stages of schizophrenia (38 females) and 67 controls (42 females) (Table 1). The inclusion criteria were as follows: The subjects were over 18 years of age and undergoing their first psychiatric hospitalisation. They were diagnosed with schizophrenia; or acute and transient psychotic disorders; and suffered from untreated psychosis for less than 24 months. Patients were medically treated upon admission, based on the recommendation of their physician. Patients suffering from psychotic mood disorders were excluded from the study.

Healthy controls over 18 years of age were recruited through advertisements unless: They had a personal history of any psychiatric disorder or had a positive family history of psychotic disorders in first- or second-degree relatives.

If a subject in either group (patient or control) had a history of neurological or cerebrovascular disorders or any MRI contraindications, they were excluded from the study.

The study was carried out in accordance with the latest version of the Declaration of Helsinki. The study design was reviewed and approved by the Research Ethics Board. Each participant received a complete description of the study and provided written informed consent.

Data were acquired at the National Centre of Mental Health in Klecany, Czech Republic. The data were acquired at the National Institute of Mental Health using Siemens MAGNETOM Prisma 3T. The acquisition parameters of T1-weighted images using MPRAGE sequence were: 240 scans; slice thickness: 0.7 mm; repetition time: 2,400 ms; echo time: 2,34 ms; inversion time: 1000 ms; flip angle: 8°, and acquisition matrix: 320 mm $\times$ 320 mm.

2.3 Preprocessing and Analysis

Prior to normative modelling, all T1 images were preprocessed using the Freesurfer v.(7.2) `recon-all` pipeline. While in the context of longitudinal analysis the longitudinal Freesurfer preprocessing pipeline is appropriate, we additionally performed cross-sectional preprocessing [18]. The reason to conduct this analysis is threefold:

First, the impact of preprocessing on the z-scores of normative models lacks prior investigation. Second, the training database of 58,000 subjects initially underwent cross-sectional preprocessing, introducing a methodological incongruity. Third, certain large-scale studies, constrained by computational resources, exclusively employ cross-sectional preprocessing. Understanding the consistency of results between the two approaches becomes crucial in such cases.

In line with [14], we performed a simple quality control procedure whereby all subjects having a rescaled Euler number greater than ten were labelled outliers and were not included in the analysis (Table 1) (see [14] and [16] for further details).

After preprocessing, patient data were projected into the adapted normative model (median Rho across all IDP was 0.3 and 0.26 for the first and the second visit, respectively—see Supp. Fig. 1). The pre-trained model used for adaptation was the `lifespan_58K_82_sites` [14]. For each subject and visit, we obtained cross-sectional z-score, as well as the underlying values needed for its computation, particularly $\varphi(y)$ and $\bar{\mathbf{w}}^T\phi(\mathbf{x})$. We conducted a cross-sectional analysis of the original z-scores to evaluate each measurement independently. We then tested for the difference in variance of the difference of the cross-sectional z-scores $z^{(2)} - z^{(1)}$ in held-out controls using Mann-Whitney U testand corrected for multiple tests using the Benjamini-Hochberg FDR correction at the 5% level of significance.

Subsequently, following (12), we derived the *z-diff* scores of change between visits. We conducted two analyses: one to investigate the group-level effect, and another to link the *z-diff* to the changes in clinical scales.

At a group-level, we identified regions with *z-diff* scores significantly different from zero using the Wilcoxon test, accounting for multiple comparisons using the Benjamini-Hochberg FDR correction.

Additionally, we performed a more traditional longitudinal analysis. As all visits were approximately one-year apart, we conducted an analysis of covariance (ANCOVA). The ANCOVA model combines a general linear model and ANOVA. Its purpose is to examine whether the means of a dependent variable (thickness in V2) are consistent across levels of a categorical independent variable (patients or controls) while accounting for the influences of other variables (age, gender, and thickness in V1). We conducted a separate test for each IDP and controlled the relevant p-values across tests using the FDR correction.

For linking the *z-diff* score to clinical change, we transformed the *z-diff* score

	Patients	**Controls**
N (% females)	98 (39%)	67 (63%)
Age, median (min, max), years	27 (18, 46)	29 (18, 54)
Interval between visits, median (min, max), years	1.1 (0.9,2.7)	1.2 (0.9, 3)
Diagnosis (only for patients)		
Schizophrenia	53	
Brief psychotic disorder	45	
Length of disease, median (min, max), months	4 (1,21)	
Clinical scales (only for patients)	**Visit 1**	**Visit 2**
PANSS sum, median (min, max)	53 (30, 94)	44 (30, 84)
PANSS Positive Symptoms, median (min, max)	11 (7, 21)	8 (7, 26)
PANSS Negative Symptoms, median (min, max)	14.5 (7, 30)	11.5 (7, 24)
GAF, median (min, max)	70 (25, 100)	80.5 (40, 98)

Table 1: Clinical description of the dataset after quality control

across all IDPs using PCA to decrease the dimensionality of the data as well as to avoid fishing. We ran PCA with 10 components and using Spearman correlation related the scores with changes in the Positive and Negative Syndrome Scale (PANSS) and Global Assessment of Functioning (GAF) scale.

3 Results

3.1 Effect of preprocessing

After obtaining cross-sectional z-scores for both types of preprocessing, we visually observed a decrease in variance between the two visits in longitudinal preprocessing compared to the cross-sectional one (Figure 2). More specifically, we calculated the mean of the difference between z-scores of V2 and V1 for each individual IDP, stratified by preprocessing and group, across all subjects. We then visualised the distribution of these means using a histogram (Figure 2C). Alternatively, we also computed the mean difference between z-scores of V2 and V1 across all IDPs for each subject, and plotted a histogram of these values. Note that this step was only done to estimate the effect of preprocessing on z-scores for further discussion. Its impact on the results is elaborated on in the discussion.

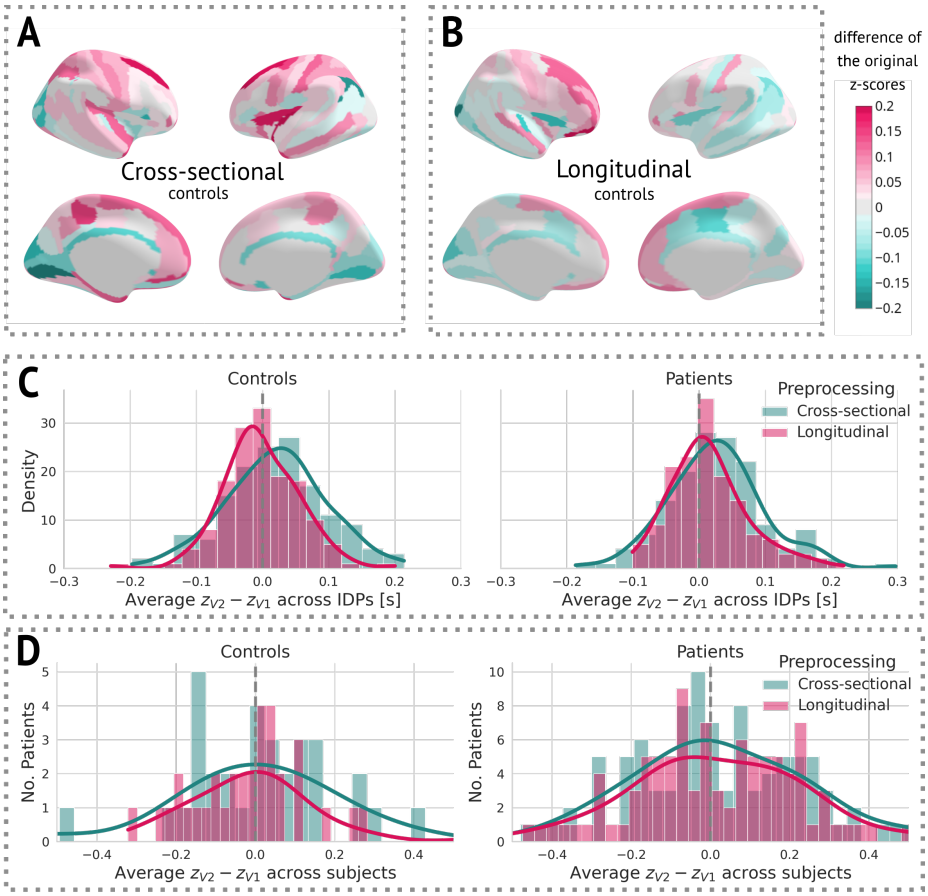

Figure 2: The effect of preprocessing across all subjects and IDPs: (A) Cross-sectional preprocessing: Heatmap of the difference of the original z-scores $(z^{(2)} - z^{(1)})$ on held-out controls. (B) Longitudinal preprocessing: Heatmap of the difference of the original z-scores $(z^{(2)} - z^{(1)})$ on held-out controls. (C) Histogram of the average $(z^{(2)} - z^{(1)})$ across all IDPs stratified by health status and preprocessing. (D) Histogram of the average $(z^{(2)} - z^{(1)})$ of each subject stratified by health status and preprocessing.

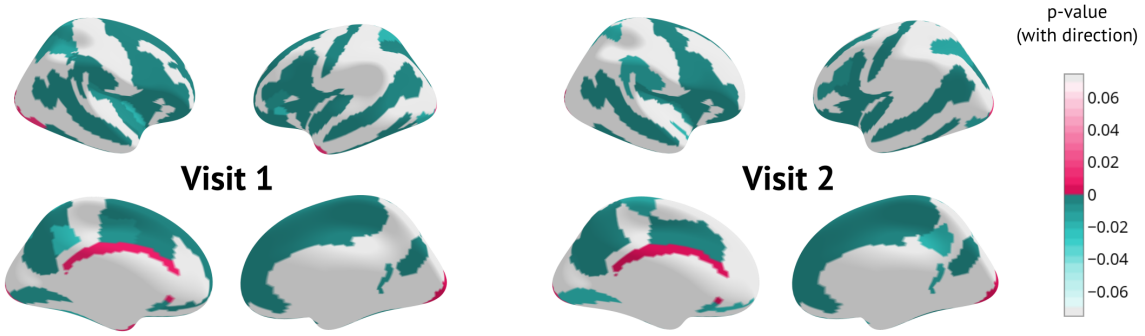

Figure 3: Cross-sectional results for each visit separately: p-values of Mann-Whitney U test between patients and held-out controls surviving Benjamini-Hochberg correction. The sign indicates the direction of change (negative means lower thickness in patients).

3.2 Cross-sectional results

At a group level, patients had significantly lower thicknesses in most areas compared to healthy populations. In particular, this difference was distinct even in the first visit, indicating structural changes prior to diagnosis (Figure 3).

3.3 Longitudinal results and patterns of change

A longitudinal analysis that evaluated the amount of structural change between the two visits showed a significant cortex normalisation of several frontal areas, namely the right and left superior frontal sulcus, the right and left middle frontal sulcus, the right and left middle frontal gyrus, and the right superior frontal gyrus (Figure 4).

In terms of linking change in clinical scores with changes in *z-diff* scores, each of the two scales was well correlated with different component. The first PCA component, which itself reflected the average change in global thickness across patients, was correlated with the change in GAF score, whereas the second component significantly correlated with the change in PANSS score (see Fig. 5).

4 Discussion

Longitudinal neuroimaging studies allow us to assess the effectiveness of interventions and gain deeper insights into the fundamental mechanisms of underlying diseases.

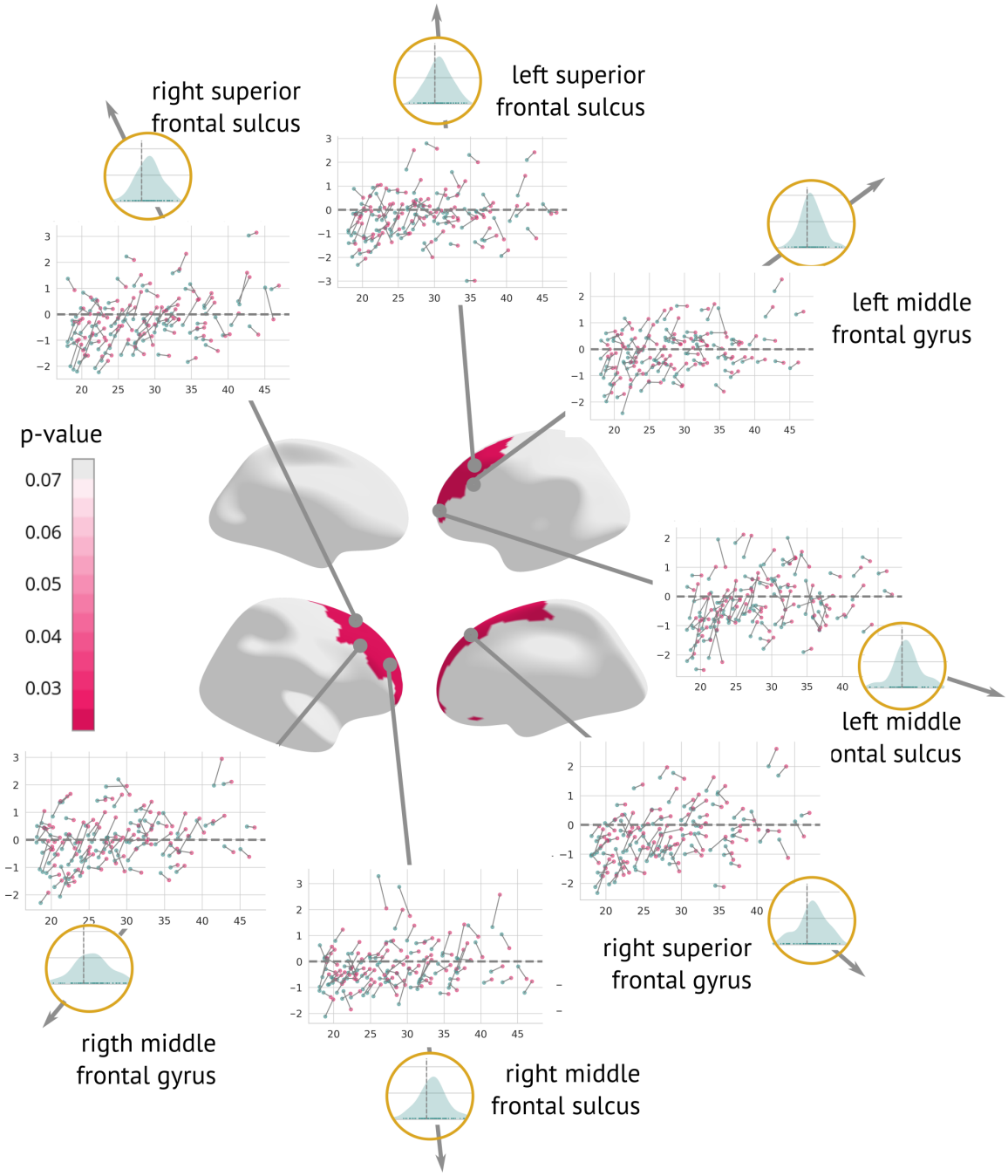

Figure 4: Regions significantly changed between the visits: Map of regions significantly changed between the two visits (centre). Each region is described using a scatterplot of z-scores across all patients for both visits (the x-axis describes age, and the y-axis depicts the z-score. Blue dots represent the first and pink dots represent the second visit). The grey dashed line highlights z=0. Histograms in the golden circles depict the distribution of the z-*diff* score.

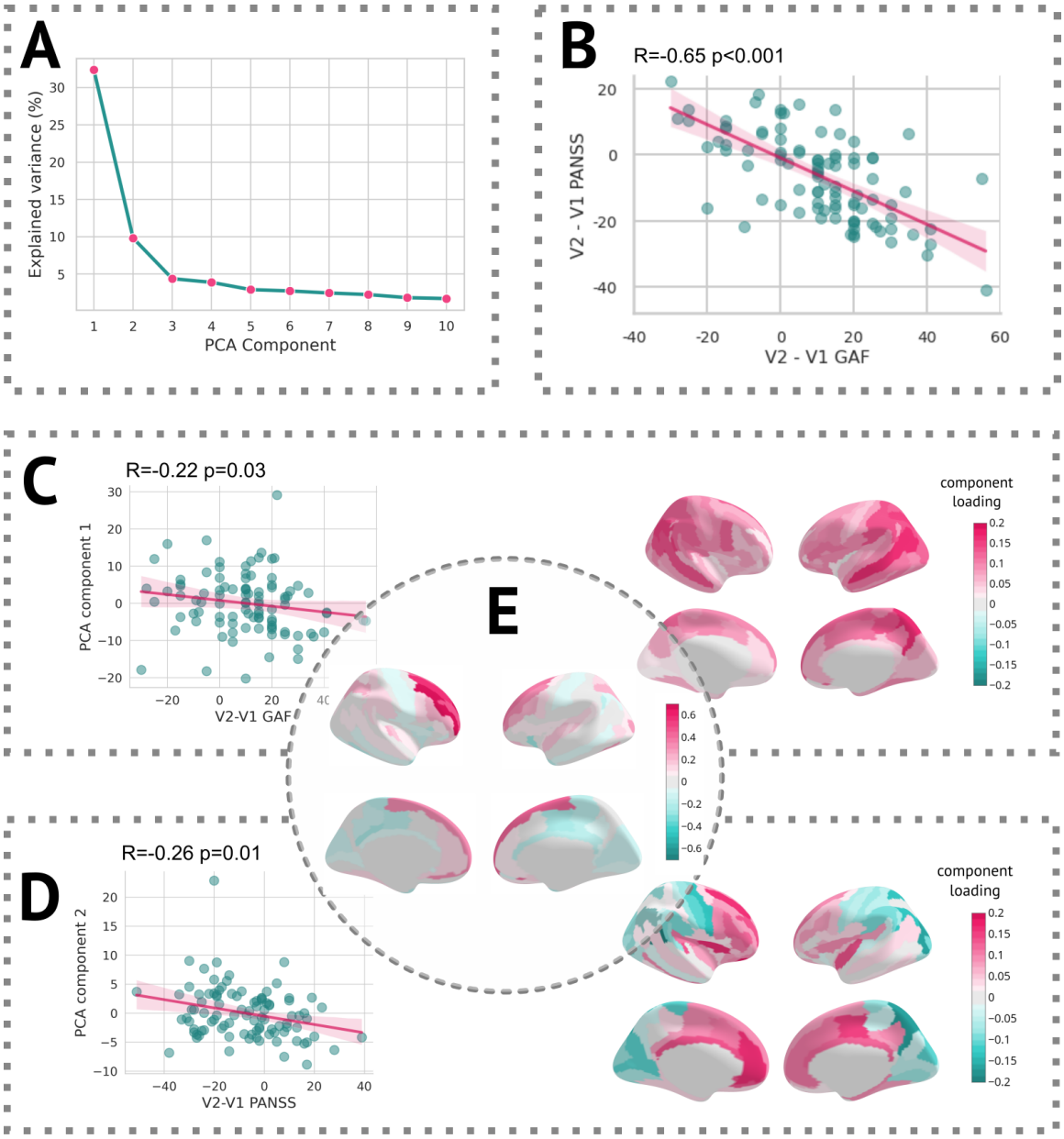

Figure 5: Results of the PCA analysis: (A) Scree plot of the explained variance of PCA components. (B) Scatterplot of change in the GAF scale vs. the change in the PANSS scale (C Left) Scatter plot of the first PCA component and difference in the GAF scale. (C Right) Heatmap of PCA loadings for the first component. (D Left) Scatter plot of the second PCA component and difference in the PANSS scale. (D Right) A Heatmap of PCA loadings for the second component. (E) Average *z-diff* score.

Despite the significant expansion of our knowledge regarding population variation through the availability of publicly accessible neuroimaging data, this knowledge, predominantly derived from cross-sectional observations, has not been adequately integrated into methods for evaluating longitudinal changes.

We propose an analytical framework that builds on normative modelling and generates unbiased features that quantify the degree of change between visits, whilst capitalising on information extracted from large cross-sectional cohorts.

4.1 Methodological contribution

Our approach is rooted in the normative modelling method based on Bayesian regression [7], the pre-trained version of which recently became available [14]. We showed that the estimation of longitudinal changes is readily available based on a preexisting cross-sectional normative model and only requires a set of healthy controls on which the variance of healthy change might be estimated. We denoted the score obtained after running the procedure as a *z-diff* score; it quantifies the extent of change between visits beyond what one would expect in the healthy population.

The core assumption of the z-diff score is that, on average, the change in healthy controls is not significant. This assumption stems from the essential idea of normative modelling that, with respect to the reference population, the position of a healthy subject does not significantly deviate over time. To verify this assumption, we used the data of 33 healthy controls which were originally used for the site-specific adaptation (for more details, see the discussion part on implementation) and computed their *z-diff* scores. After averaging these scores across all subjects, the *z-diff* score of no region was statistically significant from zero (after FDR correction). However, as pointed out by a recent work [13] studying the effect of cross-sectional normative models on longitudinal predictions, the cross-sectionally derived population centiles *by design* lack information about longitudinal dynamics. Consequently, what may appear as a population-level trajectory does not necessarily align with individual subjects' actual trajectories.

To address this limitation, our model considers the variation in individual centiles. This is achieved by estimating the impact of noise and reliability, which manifests as apparent crossings of centiles observed in healthy controls. Naturally, by incorporating this element of uncertainty, the model's ability to detect subjects who experienced

substantial changes in their trajectory over time decreases. As evident from the clinical findings, only a fraction of subjects were identified as having undergone significant changes (Supp. Fig. 2). However, at the group level, the significance of the observed changes persisted. Hence, while we adopt a cautious approach when assessing individual changes, the method still effectively identifies group-level changes.

Furthermore, unlike in [13], our approach does not aim to predict individual trajectories, but rather to quantify whether the observed changes over time exceed what would be expected.

4.2 Implementation

At the implementation level, our model requires two stages of adaptation: site-specific adaptation, as presented in [14], and a second level where we compute the variance of healthy change (noise) in healthy controls. However, if the number of longitudinal controls is limited, the site-specific adaptation may be omitted. The purpose of site-specific adaptation is to generate unbiased cross-sectional z-scores that are zero-centered with a variance of one for healthy controls. However, in the case of longitudinal analysis, the offset and normalisation constant are irrelevant since they will be identical for both visits. Therefore, the estimation of healthy change is the only essential factor in producing the *z-diff* score. Note that in this scenario, the cross-sectional result should not be interpreted.

4.3 Clinical results

Examination of the effect of preprocessing on z-scores showed that longitudinal preprocessing indeed decreases intra-subject variability compared to cross-sectional preprocessing. However, to assess the added benefit of the preprocessing, we also computed the core results (regions that significantly changed in time) for the cross-sectional data. The significant results were mostly consistent with a longitudinal pipeline: Six out of seven originally significant regions were still statistically significant (with the exception of the right middle frontal sulcus), and three other regions were labelled significant: the left superior frontal gyrus, the right inferior frontal sulcus, and the right medial or olfactory orbital sulcus (Supp. Fig. 3). Therefore, it is also possible to use cross-sectional preprocessing for longitudinal analysis; however, at a cost of increased between-visit variance and consequently decreased power (in

comparison to the longitudinal preprocessing).

The observation of cortical normalisation between the visits of early schizophrenia patients is, to a degree, counterintuitive and inconsistent with other works, which mostly report grey matter thinning. However, a meta-analysis of 50 longitudinal studies examining individuals with a heightened risk of psychosis revealed that 15 of the 19 studies indicated deviations in grey matter developmental trajectories between those with persistent symptoms and those whose symptoms resolved [19]. The authors propose that grey matter developmental trajectories may return to normal levels in individuals in the High-Risk Remitting group by early adulthood, whereas neurological irregularities may continue to advance in those whose symptoms do not resolve. Although our cohort had already received a diagnosis of schizophrenia, it is possible that early identification and treatment supported these compensatory mechanisms, as demonstrated by the normalisation of grey matter thickness in frontal regions. Notably, the affected regions also increased in raw grey matter thickness (as measured in mm, see Supp. Fig. 4).

Furthermore, we observed significant correlations between the PCA components of the *z-diff* score and changes in clinical scales, as illustrated in Fig. 5. Notably, each clinical scale exhibited distinct associations with separate PCA components, despite substantial intercorrelations (Fig. 5 (B)).

The first PCA component, which predominantly captured global changes in grey matter thickness, displayed a negative correlation with improvements in the GAF score (Fig. 5 (C)). This unexpected inverse relationship would suggest that patients who demonstrated clinical improvement over time exhibited a more pronounced decrease in grey matter thickness, as quantified by the *z-diff* score. However, further investigation revealed that this correlation was primarily driven by the patients' GAF scores in the initial visit. Specifically, the correlation between GAF scores at the first visit and the first PCA component yielded a coefficient of $R = 0.19$ ($p = 0.06$), whereas the correlation with scores at the second visit was $R = -0.10$ ($p = 0.31$). These findings suggest that lower GAF scores during the initial visit are predictive of subsequent grey matter thinning.

Conversely, the interpretation of the second PCA component, significantly correlated with changes in the PANSS score, was more straightforward (Fig. 5 (D)). The observed normalisation of grey matter thickness in frontal areas was positively correlated with improvements in the PANSS scale, indicating that symptom amelioration

was accompanied by the normalisation of grey matter thickness in these regions.

Finally, we conducted an analysis of change using conventional statistical approaches to compare the results with normative modelling. Out of 148 areas tested by ANCOVA, 6 were statistically significant. However, after controlling for multiple comparisons, no IDP persisted. This result highlights the advantages of normative models and shows improved sensitivity of our method in comparison with more conventional approaches.

4.4 Limitations

Estimating the intra-subject variability is a complex task that might be affected by acquisition and physiological noise. Assumptions must be made about the longitudinal behaviour of healthy subjects. The former problem is unavoidable, whereas the latter might be addressed by constructing longitudinal normative models. However, the project necessary for such a task would have to map individuals across their lifespan consistently. The efforts to create such a dataset are already in progress through projects like the ABCD study [20], but much more data are still needed to construct a full-lifespan longitudinal model.

Additionally, our clinical results may be affected by selection bias, where subjects experiencing a worsening of their condition dropped out of the study, whereas patients with lower genetic risk or more effective treatment continued to participate.

4.5 Conclusion

We have developed a method that utilises pre-trained normative models to detect unusual longitudinal changes in neuroimaging data. Our approach offers a user-friendly implementation and has demonstrated its effectiveness through a comprehensive analysis. Specifically, we observed significant grey matter changes in the frontal lobe of schizophrenia patients over time, surpassing the sensitivity of conventional statistical approaches. This research represents a significant advancement in longitudinal neuroimaging analysis and holds great potential for further discoveries in neurodegenerative disorders.

Acknowledgements

This research was supported by the Czech Health Research Council (NU21-08-00432); Programme Johannes Amos Comenius ('BRADY' CZ.02.01.01/00/22_008/0004643); European Research Council (grant 'MENTALPRECISION', 10100118), the Wellcome Trust under an Innovator awards ('BRAINCHART', 215698/Z/19/Z and 'PRECOGNITION', 226706/Z/22/Z), the Ministry of Education, Youth and Sports (CZ.02.2.69 /0.0/0.0/18_053/0017594); and the Czech Technical University Internal Grant Agency (SGS22/062/OHK3/1T/13).

References

[1] C. M. Williams, H. Peyre, R. Toro, and F. Ramus, "Neuroanatomical norms in the UK Biobank: The impact of allometric scaling, sex, and age," *Human Brain Mapping*, vol. 42, no. 14, pp. 4623–4642, 2021, ISSN: 1097-0193. DOI: 10.1002/hbm.25572.

[2] S. G. Heeringa and P. A. Berglund, *A Guide for Population-based Analysis of the Adolescent Brain Cognitive Development (ABCD) Study Baseline Data*, Feb. 2020. DOI: 10.1101/2020.02.10.942011.

[3] K. Franke and C. Gaser, "Ten Years of BrainAGE as a Neuroimaging Biomarker of Brain Aging: What Insights Have We Gained?" *Frontiers in Neurology*, vol. 10, 2019, ISSN: 1664-2295.

[4] C. Schuster, M. Elamin, O. Hardiman, and P. Bede, "Presymptomatic and longitudinal neuroimaging in neurodegeneration—from snapshots to motion picture: A systematic review," *Journal of Neurology, Neurosurgery & Psychiatry*, vol. 86, no. 10, pp. 1089–1096, Oct. 2015, ISSN: 0022-3050, 1468-330X. DOI: 10.1136/jnnp-2014-309888.

[5] A. F. Marquand, I. Rezek, J. Buitelaar, and C. F. Beckmann, "Understanding Heterogeneity in Clinical Cohorts Using Normative Models: Beyond Case-Control Studies," *Biological Psychiatry*, Obsessive-Compulsive Disorder, vol. 80, no. 7, pp. 552–561, Oct. 2016, ISSN: 0006-3223. DOI: 10.1016/j.biopsych.2015.12.023.

[6] R. a. I. Bethlehem *et al.*, "Brain charts for the human lifespan," *Nature*, vol. 604, no. 7906, pp. 525–533, Apr. 2022, ISSN: 1476-4687. DOI: 10.1038/s41586-022-04554-y.

[7] C. J. Fraza, R. Dinga, C. F. Beckmann, and A. F. Marquand, "Warped Bayesian linear regression for normative modelling of big data," *NeuroImage*, vol. 245, p. 118 715, Dec. 2021, ISSN: 1053-8119. DOI: 10.1016/j.neuroimage.2021.118715.

[8] M. Habes *et al.*, "The Brain Chart of Aging: Machine-learning analytics reveals links between brain aging, white matter disease, amyloid burden, and cognition in the iSTAGING consortium of 10,216 harmonized MR scans," *Alzheimer's & Dementia*, vol. 17, no. 1, pp. 89–102, 2021, ISSN: 1552-5279. DOI: 10.1002/alz.12178.

[9] W. H. L. Pinaya *et al.*, "Using normative modelling to detect disease progression in mild cognitive impairment and Alzheimer's disease in a cross-sectional multicohort study," *Scientific Reports*, vol. 11, no. 1, p. 15 746, Aug. 2021, ISSN: 2045-2322. DOI: 10.1038/s41598-021-95098-0.

[10] T. Wolfers *et al.*, "Replicating extensive brain structural heterogeneity in individuals with schizophrenia and bipolar disorder," *Human Brain Mapping*, vol. 42, no. 8, pp. 2546–2555, 2021, ISSN: 1097-0193. DOI: 10.1002/hbm.25386.

[11] M. Zabihi *et al.*, "Dissecting the Heterogeneous Cortical Anatomy of Autism Spectrum Disorder Using Normative Models," *Biological Psychiatry: Cognitive Neuroscience and Neuroimaging*, The Bridging of Scales: Techniques for Translational Neuroscience, vol. 4, no. 6, pp. 567–578, Jun. 2019, ISSN: 2451-9022. DOI: 10.1016/j.bpsc.2018.11.013.

[12] A. F. Marquand, S. M. Kia, M. Zabihi, T. Wolfers, J. K. Buitelaar, and C. F. Beckmann, "Conceptualizing mental disorders as deviations from normative functioning," *Molecular Psychiatry*, vol. 24, no. 10, pp. 1415–1424, Oct. 2019, ISSN: 1476-5578. DOI: 10.1038/s41380-019-0441-1.

[13] M. A. Di Biase *et al.*, "Mapping human brain charts cross-sectionally and longitudinally," *Proceedings of the National Academy of Sciences*, vol. 120, no. 20, e2216798120, May 2023. DOI: 10.1073/pnas.2216798120.

[14] S. Rutherford *et al.*, "Charting Brain Growth and Aging at High Spatial Precision," Cold Spring Harbor Laboratory, Tech. Rep., Aug. 2021, ch. New Results, p. 2021.08.08.455487. DOI: 10.1101/2021.08.08.455487.

[15] T. Cole, "The development of growth references and growth charts," *Annals of Human Biology*, vol. 39, no. 5, pp. 382–394, Sep. 2012, ISSN: 0301-4460. DOI: 10.3109/03014460.2012.694475.

[16] S. M. Kia *et al.*, "Closing the life-cycle of normative modeling using federated hierarchical Bayesian regression," *PLOS ONE*, vol. 17, no. 12, e0278776, 2022, ISSN: 1932-6203. DOI: 10.1371/journal.pone.0278776.

[17] F. Spaniel *et al.*, "Altered Neural Correlate of the Self-Agency Experience in First-Episode Schizophrenia-Spectrum Patients: An fMRI Study," *Schizophrenia Bulletin*, vol. 42, no. 4, pp. 916–925, Jul. 2016, ISSN: 0586-7614. DOI: 10.1093/schbul/sbv188.

[18] M. Reuter, N. J. Schmansky, H. D. Rosas, and B. Fischl, "Within-subject template estimation for unbiased longitudinal image analysis," *Neuroimage*, vol. 61, no. 4, pp. 1402–1418, Jul. 2012, ISSN: 1053-8119. DOI: 10.1016/j.neuroimage.2012.02.084.

[19] K. Merritt, P. Luque Laguna, A. Irfan, and A. S. David, "Longitudinal Structural MRI Findings in Individuals at Genetic and Clinical High Risk for Psychosis: A Systematic Review," *Frontiers in Psychiatry*, vol. 12, 2021, ISSN: 1664-0640.

[20] B. J. Casey *et al.*, "The Adolescent Brain Cognitive Development (ABCD) study: Imaging acquisition across 21 sites," *Developmental Cognitive Neuroscience*, The Adolescent Brain Cognitive Development (ABCD) Consortium: Rationale, Aims, and Assessment Strategy, vol. 32, pp. 43–54, Aug. 2018, ISSN: 1878-9293. DOI: 10.1016/j.dcn.2018.03.001.

Supplement

Posterior predictive distribution for difference between visits

Here we derive the posterior predictive distribution for the difference $\varphi(y^{(2)}) - \varphi(y^{(1)})$. The argument is standard. Denote $\Delta_{\mathbf{x}} = \phi(\mathbf{x}^{(2)}) - \phi(\mathbf{x}^{(1)})$ and $\Delta_y = \varphi(y^{(2)}) - \varphi(y^{(1)})$. Since $\Delta_{\mathbf{x}}^T \mathbf{w} | \mathbf{x}^{(1)}, \mathbf{x}^{(2)}; \mathbf{y}, \mathbf{\Phi}; \alpha, \beta, \boldsymbol{\gamma} \sim \mathcal{N}(\Delta_{\mathbf{x}}^T \bar{\mathbf{w}}, \Delta_{\mathbf{x}}^T \mathbf{A}^{-1} \Delta_{\mathbf{x}})$ and $\Delta_y | \mathbf{x}^{(1)}, \mathbf{x}^{(2)}; \mathbf{w} \sim \mathcal{N}(\Delta_{\mathbf{x}}^T \mathbf{w}, 2\sigma_\xi^2)$, the posterior predictive density is

$$
\begin{aligned}
&f(\Delta_y | \mathbf{x}^{(1)}, \mathbf{x}^{(2)}; \mathbf{y}, \mathbf{\Phi}; \alpha, \beta, \boldsymbol{\gamma}) = \\
&\quad = \int f_{\mathcal{N}(\Delta_{\mathbf{x}}^T \mathbf{w}, 2\sigma_\xi^2)}(\Delta_y | \mathbf{x}^{(1)}, \mathbf{x}^{(2)}; \mathbf{w}) \cdot f_{\mathcal{N}(\Delta_{\mathbf{x}}^T \bar{\mathbf{w}}, \Delta_{\mathbf{x}}^T \mathbf{A}^{-1} \Delta_{\mathbf{x}})}(\Delta_{\mathbf{x}}^T \mathbf{w} | \mathbf{x}^{(1)}, \mathbf{x}^{(2)}; \mathbf{y}, \mathbf{\Phi}; \alpha, \beta, \boldsymbol{\gamma}) \, \mathrm{d}(\Delta_{\mathbf{x}}^T \mathbf{w}) \\
&\quad = \int f_{\mathcal{N}(0, 2\sigma_\xi^2)}(\Delta_y - \Delta_{\mathbf{x}}^T \mathbf{w} | \mathbf{x}^{(1)}, \mathbf{x}^{(2)}; \mathbf{w}) \cdot f_{\mathcal{N}(\Delta_{\mathbf{x}}^T \bar{\mathbf{w}}, \Delta_{\mathbf{x}}^T \mathbf{A}^{-1} \Delta_{\mathbf{x}})}(\Delta_{\mathbf{x}}^T \mathbf{w} | \mathbf{x}^{(1)}, \mathbf{x}^{(2)}; \mathbf{y}, \mathbf{\Phi}; \alpha, \beta, \boldsymbol{\gamma}) \, \mathrm{d}(\Delta_{\mathbf{x}}^T \mathbf{w}).
\end{aligned}
$$

This has the familiar convolution form of the densities of $\mathcal{N}(0, 2\sigma_\xi^2)$ and $\mathcal{N}(\Delta_{\mathbf{x}}^T \bar{\mathbf{w}}, \Delta_{\mathbf{x}}^T \mathbf{A}^{-1} \Delta_{\mathbf{x}})$. It is known to produce the density of $\mathcal{N}(\Delta_{\mathbf{x}}^T \bar{\mathbf{w}}, \Delta_{\mathbf{x}}^T \mathbf{A}^{-1} \Delta_{\mathbf{x}} + 2\sigma_\xi^2)$ (by completion to squares in the exponent).

Quality of fit across regions of interest

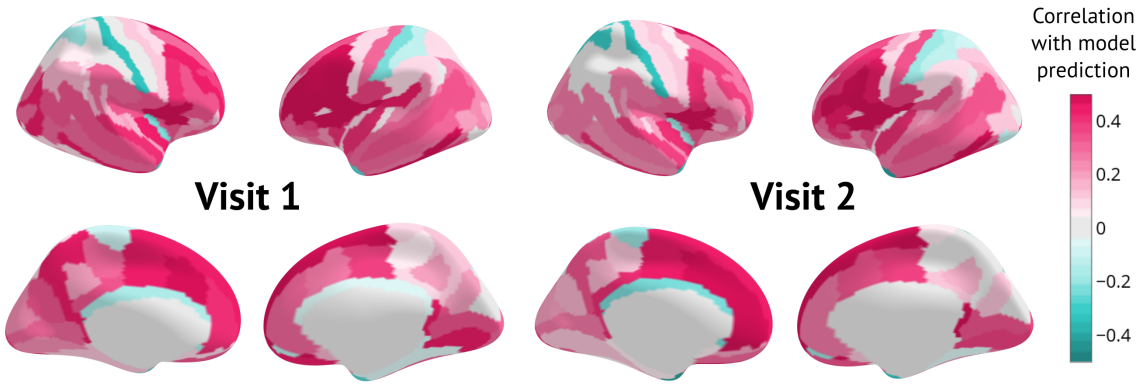

Supplementary Figure 1: **Quality of fit as measured by Rho for the first and the second visit.**

Comparison of preprocessing

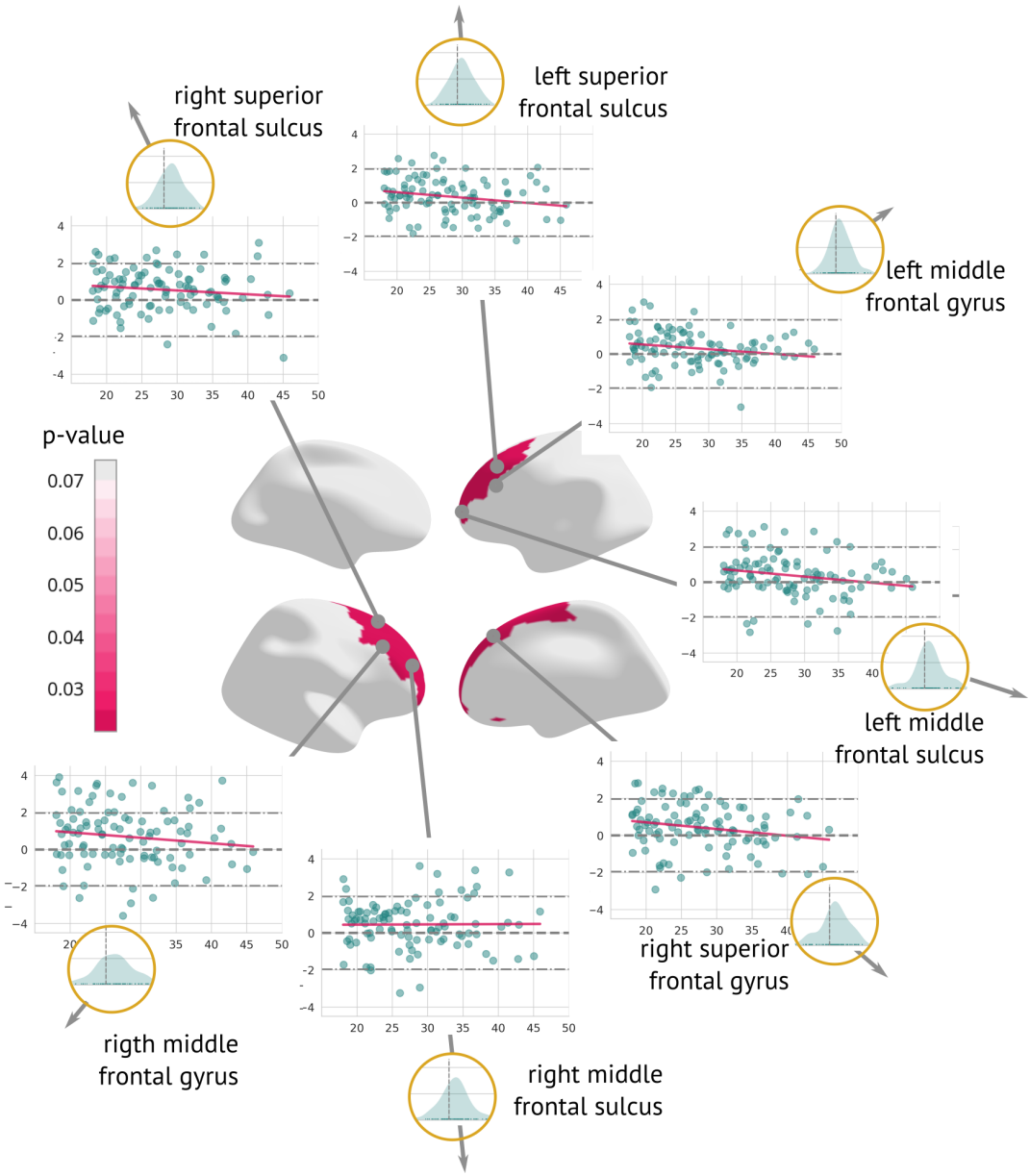

Supplementary Figure 2: Regions significantly changed between the visits (longitudinal preprocessing): Map of regions significantly changed between the two visits (centre). Each region is described using a scatterplot of *z-diff* across all patients for both visits (the x-axis describes age, and the y-axis depicts the *z-diff*. Blue dots represent individual patients and the pink line shows a trend of *z-diff* change). The Grey dashed line highlights z=0. Histograms in the golden circles depict the distribution of the *z-diff* score.

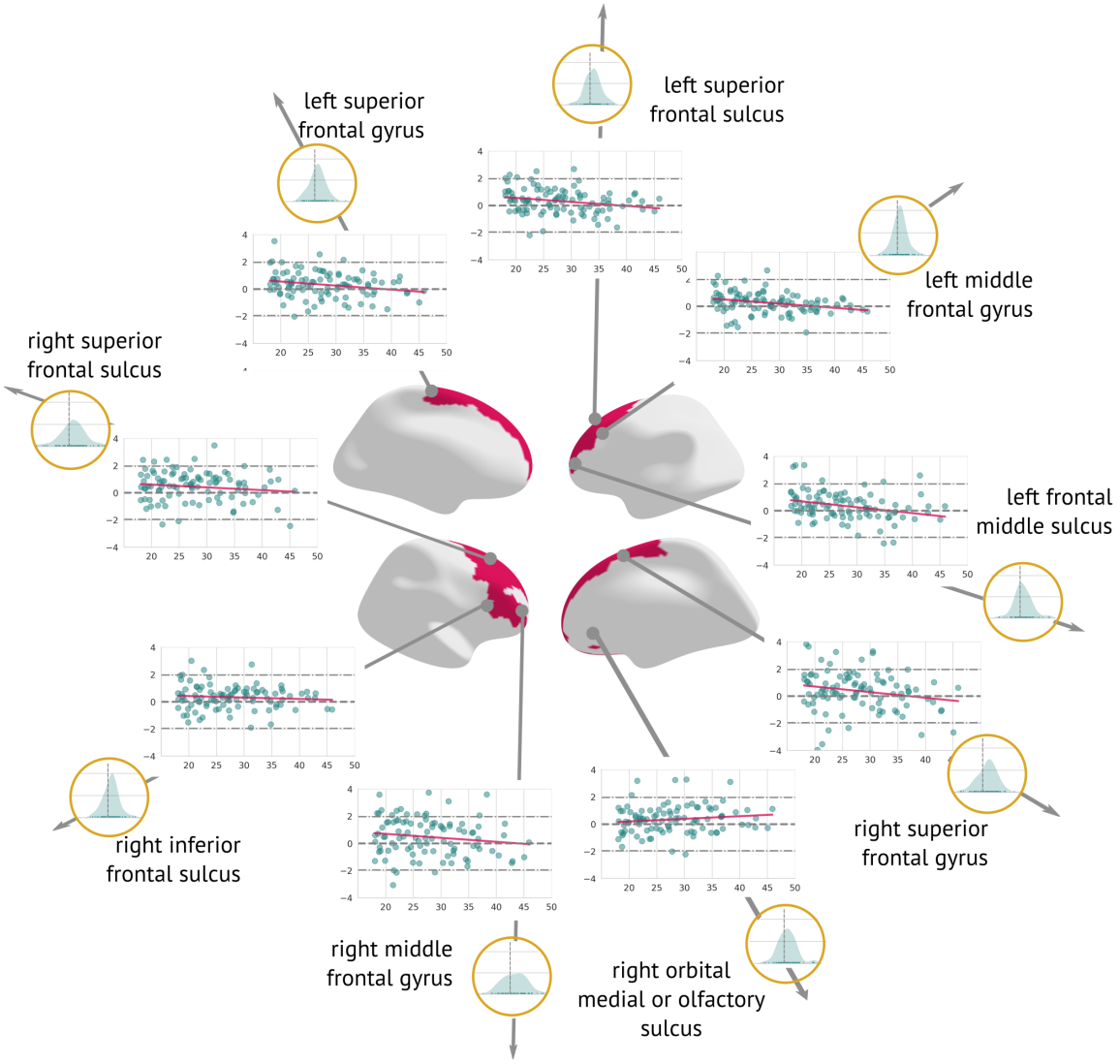

Supplementary Figure 3: Regions significantly changed between the visits (cross-sectional preprocessing): Map of regions significantly changed between the two visits (centre). Each region is described using a scatterplot of *z-diff* scores across all patients for both visits (the x-axis describes age, and the y-axis depicts the *z-diff* score. The grey dashed line highlights z=0. Histograms in the golden circles depict the distribution of the *z-diff* score.

Raw changes observed in significant regions

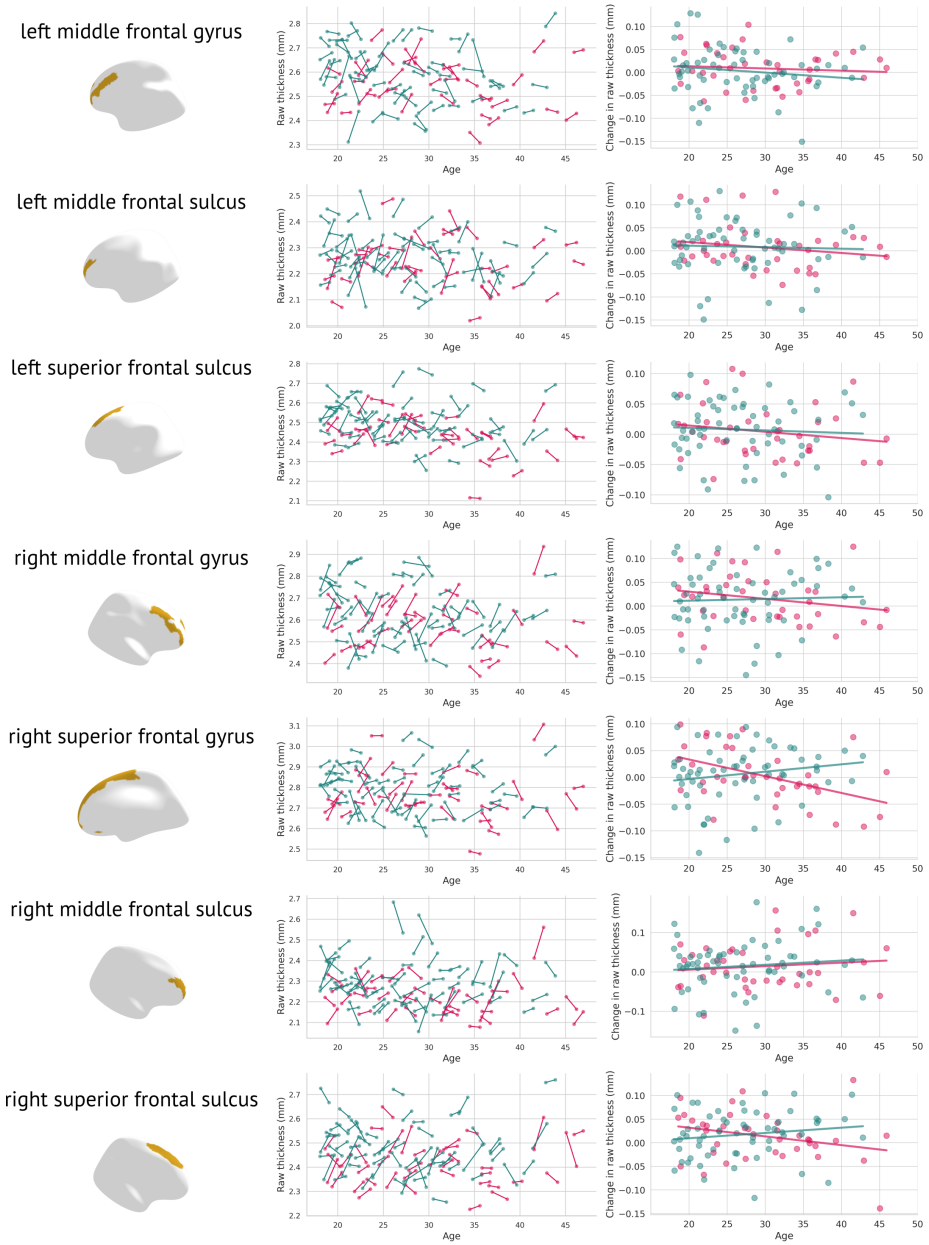

Supplementary Figure 4: Raw changes in grey matter thickness: Each significantly changed region is presented twice, once as a scatter plot containing the original grey matter thickness for both visits (left); females are plotted in pink, males in blue. The figure on the right depicts V2-V1 in raw thicknesses (separately for females – pink, and males – blue).